

# **CHARACTERIZATION OF NANOPOROUS SYSTEMS WITH LOW FIELD NMR: APPLICATION TO KAOLINITE AND SMECTITE CLAYS**

M. Fleury, S. Gautier, F. Norrant, E. Kohler  
IFP Energies nouvelles, 1 avenue de Bois-Préau, 92852 Rueil-Malmaison, France.

*This paper was prepared for presentation at the International Symposium of the Society of Core Analysts held in Austin, Texas, USA 18-21 September, 2011*

## **ABSTRACT**

Nuclear Magnetic Resonance (NMR) relaxation techniques are able to detect very small pore sizes, down to nano-meter length scales. We focus here on the characterization of clays and specifically the interlayer spacing present in some types of clays such as smectites and we studied two types of model clays: kaolinite and montmorillonite. Contrary to kaolinite, montmorillonite contains a large amount of interlayer water. Powders and compacted disks were equilibrated at a relative humidity of 100% during three weeks. Their water content was varied by drying at 100°C, and at laboratory relative humidity (40-50%). Powder samples were also prepared with ethylene glycol, a larger molecule able to replace and fill the interlayer space. Different NMR measurements were performed at a magnetic field of 0.5T (proton Larmor frequency of 23.7 MHz): (i) the standard CPMG sequence, (ii) 2D  $T_1$ - $T_2$  sequence to analyze the mobility of protons and relate  $T_1$  and  $T_2$  peaks in multimodal distribution (iii) a free induction decay (FID) sequence.

The  $T_2$  transverse relaxation times are usually multimodal with very short components ( $T_2 < 50 \mu\text{s}$ ) representing hydroxyls part of the clay crystallographic lattice. Using a combination of FID and CPMG, the amount of hydroxyls agrees reasonably well with the value calculated from the structural formulae obtained from X ray diffraction measurements. At a relative humidity of 100%, kaolinite has a relaxation time of 6 ms, much larger than smectite (1 ms) due to the very large difference of specific surface area. For smectite, the interlayer water is in fast exchange with surface water and cannot be identified at ambient temperature, except when the powder is equilibrated with ethylene glycol, in which case two relaxation modes are present. From freezing experiments, we evaluated an inter-layer relaxation time  $T_2$  of 0.6 ms. At RH=100%, 80% of the detected water is located in the interlayer space, in agreement with published results.

## **INTRODUCTION**

NMR is one of the few techniques, along with cation exchange capacity, able to characterize clays in their wet state, contrary to helium or mercury intrusion techniques. For the determination of the so-called "Clay Bound Water", a confusing denomination, it has been used for many years to separate the "effective" from the total porosity in logging data, with important impacts in terms of reservoir appraisal. The study of clays is too

difficult when present in a sandstone for example and it is much more convenient to deal with clay powders with a well defined structure. Matteson et al. [1] studied 4 types of clay slurries (kaolinite, smectite, illite and glauconite) to determine whether NMR relaxation measurements could distinguish these clays and if a true clay bound water peak can be identified. The results show mostly unimodal  $T_2$  distribution with the peak position depending on compaction without clear difference between the different types of clay studied. Interestingly, the calculated surface relaxivity  $\rho_2$  are around  $2 \mu\text{m/s}$ , weakly depending on iron content. Clearly, the small relaxation time in clays is due to a high specific surface area and not to a high surface relaxivity induced by paramagnetic impurities. Hence, the length scales that can be explored with NMR relaxation according to the standard fast diffusion model reaches easily the nm length scales and less, most standard low field instruments being able to catch relaxation time as short as 0.1 ms. In addition, with such values of surface relaxivities, relaxation times much smaller than about 0.5 ms do not exist in the framework of the fast diffusion model. Indeed, the lowest measurable relaxation time is the surface relaxation time  $T_{2s} = \epsilon / \rho_2 \cong 0.5 \text{ ms}$  corresponding to spin bearing molecules permanently relaxing at the solid surface (but not adsorbed), where  $\epsilon$  is the thickness of the water layer at the solid surface in which molecules diffuse, of the order of 1 nm or less.

The interlayer spacing in swelling clays is a porosity compartment with specific properties (see Michot et al. [2] for a review). For example, Raynal and Jullien [3] showed that the water density must be significantly higher ( $1.2 \text{ g/cm}^3$ ) than bulk values to explain simple helium porosity measurements on clay powders at different relative humidity. In principle, we expect to be able to distinguish interlayer water from external water with NMR techniques because of the small but variable spacing of the interlayer, around 1 nm. However, the mobility of the water in the interlayer, the time scale of exchange with external water and their respective volume fraction is a key for its observation. Water may have a reduced or no mobility because it can be bonded to the interlayer cations that balances the layer negative charge; we also expect a dependence of the mobility with the type of cations. Concerning the volume fraction, Ben Rhaiem [4] estimated a fraction of 85 % for the external water in a Wyoming Ca-montmorillonite at a relative humidity of 99.9%. Hence there is a significant volume fraction of internal water, making possible the detection of internal water with low field NMR techniques. This was clearly evidenced by Chitale et al. [5] who matched closely the water content of montmorillonites with NMR data and indicated a relaxation time around 1 ms. However, Montavon et al. [6] found that external and internal water could not be distinguished due to the fast exchange between these two proton populations, except at low temperature ( $-25^\circ\text{C}$ ) when external water is frozen. In addition, there exist a third type of protons detected by NMR, namely structural protons (hydroxyls) which are part of the solid structure [6]. Fortunately, the range of relaxation for these protons is extremely short, around  $50 \mu\text{s}$ , in principle not superimposed to water protons.

The objective of this work is to clarify the NMR interpretation in natural but well defined clays. We studied two types of clays, namely kaolinite and smectite, in order to compare

the NMR response with and without inter layer water. The water content of the samples is modified by varying the relative humidity (100% and ambient), and the temperature up to 100°C to obtain a dry state. The temperature was varied down to -60°C in order to freeze external water and identify internal water. Samples were also immersed in deuterium to observe possible exchange.

## MATERIALS AND NMR METHODS

### Clay samples and preparation

We used two clay types, one without interlayer water (kaolinite) and a natural smectite (Table 1). For smectite, the starting clay mineral for this experimental study was natural smectite coming from Libya. XRD analysis for the natural clay revealed dioctahedral smectite with an interlayer distance at 1.254 nm (at 50% RH) and 0.149 nm for (060) parameter. Cell refinement calculation conduct to a cell volume equals to 0.576 nm<sup>3</sup> with these cell parameters (space group: C 2/m): a=0.519, b=0.894, c=1.261 and  $\alpha=\gamma=90^\circ$ ,  $\beta=99.85^\circ$ . XRD analysis also revealed two soluble minerals: calcite and dolomite. The total amount of impurities is estimated to be lower than 5%. Measurement of smectite CEC, according to Copper Ethylenediamine Complex method [7] equals to 78 meq/100g. Numerical decomposition of FTIR spectrum which allows exploring octahedral chemistry [8, 9], associated to CEC and XRD measurement (an occupancy of two octahedral cations per formula unit according to measurement at 1,5Å of 060 X-ray diffraction peak) permit to obtain a global structural formulae (considering no vacancy substitutions):



X-ray pattern inversion constrained by the structural formulae show that the interlayer space of natural smectite is composed by Na and Ca (respectively 2/3 and 1/3).

For kaolinite, the powder originates from the collection of the Clay Minerals Society. This kaolin is a well-crystallized clay (Washington County, Georgia) described by Pruett and Webb. X-ray diffraction analysis does not show the presence of accessory minerals and can be seen that the sample is pure. Cell refinement calculation conduct to a cell volume equals to 0.164 nm<sup>3</sup> with these cell parameters (space group: C1): a=0.515, b=0.514, c=0.739 and  $\alpha=84,18^\circ$ ,  $\beta=75.25^\circ$  and  $\gamma=60.22^\circ$ . The structural formulae is



Fully hydrated clay powders were prepared by equilibrating the powders at 100% water relative humidity (RH) in a closed vessel containing water during 3 weeks at ambient laboratory temperature. Then, part of the powder was taken in a new vessel and water was further exchanged with ethylene glycol (C<sub>2</sub>H<sub>6</sub>O<sub>2</sub>) by letting the powders equilibrate with this liquid again. Ethylene glycol has a high affinity for water and will replace all water molecules present in the sample, including interlayer water. While about at least 3 layers of water can be stacked within the interlayer spacing, ethylene glycol is a larger molecule and will have a different configuration, roughly with a single molecular layer occupying the interlayer spacing [10]. Ethylene glycol is also more viscous than water (16 cP at 25 °C, specific density 1.1 kg/m<sup>3</sup>), thus reducing in the same proportion the

self-diffusion coefficient and consequently the exchange time between external and internal water. Compacted clay discs of diameter 15 mm and thickness around 8 mm were obtained by compressing at 9t during 1h powder clays at ambient humidity. Then, the powders and disks were hydrated at RH=100% in a closed vessel.

Table 1: specific surface properties of the clay used in this study

Specific surface (m <sup>2</sup> /g)		Smectite	Kaolinite
External	Basal	93	10-30
	lateral	11	
Interlayer		657	

### NMR methods

The experiments have been carried out on a Maran Ultra proton spectrometer from Oxford Instruments with a proton Larmor frequency of 23.7 MHz. Standard free induction decay (FID) and transverse magnetization CPMG decay curves were measured. When needed, we used a modified CPMG sequence in which the inter-echo time is initially set at the lowest possible and then increased gradually up to 100  $\mu$ s or more in order to catch at the same time very short and very long relaxation times. This is the case in deuterium exchange experiments. 2D  $T_1$ - $T_2$  maps were determined using an inversion recovery sequence followed by a CPMG sequence:

$$P_{180} - \tau_1 - P_{90} - (\tau - P_{180} - \text{echo})_n$$

where  $\tau_1$  takes usually 40 discrete values spaced logarithmically, and the number of echo  $n$  is adjusted in order to reach zero signal (noise level). Hence, we obtain a magnetization function of two times,  $\tau_1$  and  $n\tau$ , later analyzed in terms of a  $T_1$ - $T_2$  2D map computed with an in-house 2D inverse Laplace transform software. In the present situation, the ratio  $T_1/T_2$  can be used as an indication of the proton mobility: indeed for solid protons, we expect a high  $T_1/T_2$  ratio (10 or more) whereas for protons carried by diffusing molecules, a  $T_1/T_2$  of about 2 is expected (at the low field considered here).

Table 2: Main characteristics of the NMR instrument. P90 is the 90° pulse duration.

Probe diameter (mm)	Probe dead time ( $\mu$ s)	P90 ( $\mu$ s)	Filter dead time 100kHz/1MHz ( $\mu$ s)	$\tau$ spacing ( $\mu$ s)	1 <sup>st</sup> FID ( $\mu$ s)
10	5	2	15	25	21
			5	15	11
18	15	6	15	30	33

We used two NMR probes of diameter 10 and 18 mm depending on the desired information and size of samples. The capacity of detecting "solid like protons" with very short relaxation times depends critically on the probe dead time. Using a small probe diameter of 10 mm reduces significantly the dead time down to 5  $\mu$ s compared to the standard 18 mm probe (Table 2). It also reduces the 90° pulse duration to insure a larger frequency bandwidth when detecting solid protons. In addition, the filter dead time can be reduced significantly using a 1 MHz bandwidth, at the expenses however of the signal

to noise ratio. Note that the smallest  $\tau$  spacing available is 15  $\mu\text{s}$  and hence, the first acquired point in the CPMG decay is at 30  $\mu\text{s}$ .

When necessary, the magnetization decays obtained from FIDs were analyzed using gaussian decays instead of exponential functions according to:

$$M(t) = \sum_i A_i \exp\left[-\left(\frac{t}{T_{2i}^*}\right)^2\right] \quad (1)$$

where both the amplitude  $A_i$  and time  $T_{2i}^*$  are fitted using standard optimization routines without any regularization parameter (only a few components are used). Gaussian decays are applicable to the magnetization decays of "solid" protons. For CPMG sequences, the magnetization decay is analyzed using exponential functions according to:

$$M(t) = \sum_i A_i \exp\left(-\frac{t}{T_{2i}}\right) \quad (2)$$

The smallest relaxation time that can be determined is of the order of the inter-echo time  $2\tau$  that varies with the probe and experimental parameter used. Indeed, if  $T_2=2\tau$ , the first point recorded in the magnetization decay is at  $2\tau$  and attenuated by a factor  $1/e=0.37$ . Hence, the amplitude  $A_i$  calculated by our Laplace Inverse program for relaxation times smaller than about  $2\tau$  should not be interpreted quantitatively but only qualitatively, i.e. the CPMG magnetization curve contain fast decays but it cannot be known precisely how many protons are in this range. In addition, the hypothesis of exponential decays for very small relaxation time is doubtful because they can be below the theoretical surface relaxation time inferred from standard fast exchange models. In both gaussian and exponential cases, the total (extrapolated) magnetization  $M_0=M(t=0)$  is then obtained from the sum of the amplitudes  $A_i$ . The variable temperature experiments were performed using a nitrogen flow around the NMR tube (set-up of Oxford Instrument) using the 18 mm probe. To decrease the temperature down to -60 °C, liquid nitrogen was used to lower the gas flow temperature enough before the regulating heating resistance placed close to the NMR tube. The temperature of the sample was measured continuously during the experiment at the top of the powder using an optical system. We measured a temperature gradient of about 1.5 °C between the bottom and top of the sample.

## RESULTS

### Comparison between compacted and powder clays

Our study initially started with compacted clay discs in order to reproduce or approach natural situations. We show here that the study of powders provides similar information. Indeed, the NMR relaxation time distributions obtained on powder and discs (RH=100%) are very similar (Figure 1). For kaolinite, external water signal located around 2 ms are identical whereas structural protons around and below 0.1 ms are clearly well separated. For smectite, there exist in both cases a dominating peak at 0.5 ms. Further details about the interpretation of the different peaks will be given later. Interestingly, we can calculate the porosity and saturation of the discs using the following formulas:

$$\Phi = 1 - \frac{V_S}{V_T} \quad \text{with} \quad V_S = \frac{m_S - m_W}{d} \quad S_W = \frac{V_W}{V_P} = \frac{V_W}{V_T - V_S} \quad (3)$$

where  $V_S$  is the solid volume calculated from the measured mass  $m_S$  of the sample and the measured mass  $m_W$  of water in the sample (from NMR),  $V_T$  is the total geometric volume (calculated from the measured diameter and length),  $V_W$  is the measured volume of water from NMR and  $d$  is the specific density of the solid assumed to be  $2.70 \text{ g/cm}^3$ . For kaolinite, we found  $\Phi=41\%$  and  $S_W=11\%$  and for smectite,  $\Phi=23\%$  and  $S_W=78\%$ .

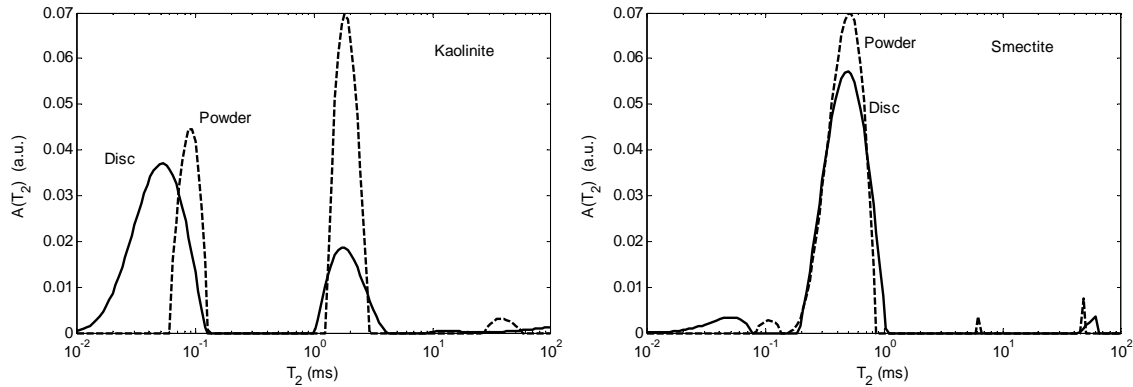


Figure 1: Comparison of the  $T_2$  distribution obtained on the powders and compacted discs at a relative humidity of 100 %, for kaolinite and smectite.

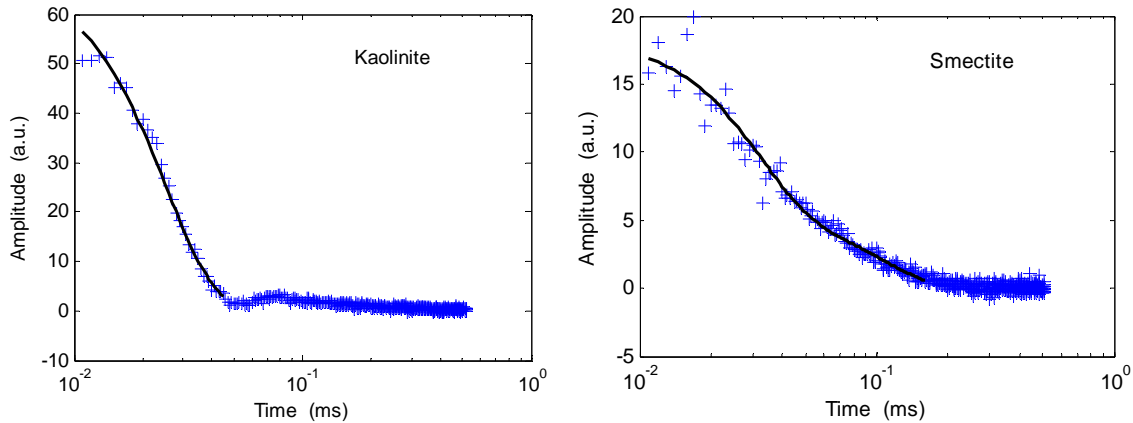


Figure 2: FID signals (10 mm NMR probe) characterizing structural protons measured on kaolinite and smectite powders after heating at  $100^\circ\text{C}$ . The lines indicate the fit with gaussian functions; for kaolinite:  $A_1=68$ ,  $T_{21}^*=25\mu\text{s}$ ; for smectite:  $A_1=12.6$ ,  $T_{21}^*=32\mu\text{s}$ ,  $A_2=5.7$ ,  $T_{22}^*=103\mu\text{s}$ .

### Structural protons calculations

We used the powder samples dried at  $100^\circ\text{C}$  to evaluate the number of protons part of the structure (OH groups). For these samples, CPMG relaxation times are below 0.1 ms and FID signals must be used (Figure 2), using gaussian functions to describe the magnetization decay, as mentioned in the previous section. With the 10 mm NMR probe

and large bandwidth filter, the FID decays can be recorded starting 10  $\mu$ s after the end of the 90° pulse and we can make reasonable estimates of the amplitude at zero time, i.e. the number of protons in the sample. According to the structural formulas, the mass of hydrogen  $m_H$  deduced from the measured mass  $m_S$  of the sample for smectite and kaolinite is respectively  $m_H=2/365.9 m_S$  and  $m_H=2/129 m_S$ . Calibrating further the signal using a known mass of water, we can then compare the measurements to the theory. For kaolinite, we measured  $m_H=2.0$  mg whereas the predicted value is 1.9 mg. Taking the first point of the FID instead of the extrapolated value yields a measured value of 1.5 mg. For smectite, the measured value is 0.54 mg and the predicted one is 0.68 mg. For this sample, the amount of structural protons is about 3 times smaller and the signal is more noisy. The reasonable agreement between the measured and predicted values confirm that the observed signals can be associated with structural protons.

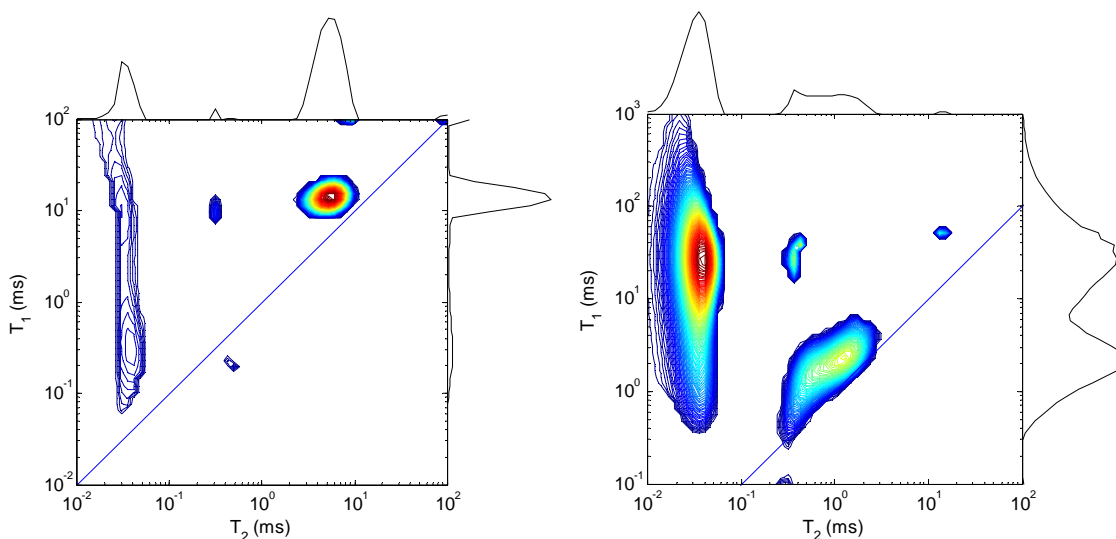


Figure 3:  $T_1$ - $T_2$  maps obtained on kaolinite powders at 100 % relative humidity using water (left) and ethylene glycol (right).

### Kaolinite

The  $T_2$  distributions obtained on kaolinite at 100% relative humidity is typically bimodal (Figure 3 left); the dominant peak is located at about 5 ms ( $T_1/T_2 \cong 1.5$ ), and the second one is at the limit of resolution ( $T_1/T_2 < 100$ ). Clearly, the  $T_1$  distributions alone are not very useful because the variable  $T_1/T_2$  ratio indicating a different proton mobility. In this case, there is no interlayer porosity and the dominant peak can be associated with surface (external) water. The  $T_1$ - $T_2$  map clearly confirm such interpretation: the dominant  $T_2$  peak has an expected  $T_1/T_2$  ratio around 1.5, while this ratio increases up to 100 for the lowest mode. When water is replaced by ethylene glycol, the bimodal signature is still present but the dominant peak is now located at the limit of resolution (0.04 ms) and the second mode is around 1 ms (Figure 3 right). As will be seen later with the quantitative

evaluation, there is less ethylene glycol at the surface (the adsorption isotherms are different) resulting also in a smaller relaxation time.

Two additional experiments were performed for a further demonstration of the above interpretation of the different parts of the NMR  $T_2$  distributions. First, the kaolinite powder was immersed in deuterium ( $D_2O$ ) to verify the expected lack of exchange of hydroxyls that are part of the crystallographic lattice (in fact, it is certainly possible to deuterate the surface but at a higher temperature). Indeed, the peak at 0.06 ms does not vary as the powder becomes a suspension in  $D_2O$  (Figure 4). The distribution becomes trimodal, the middle peak corresponding to water between the clay particles, and the peak at 10 s corresponding to water in the supernatant, mixture of  $H_2O$  and  $D_2O$  (bulk  $H_2O$  diluted into  $D_2O$  relaxes at a time larger than bulk pure water due to the formation H-O-D molecules with different NMR properties). In the second experiment, we lowered the temperature of the sample in order to freeze the surface water (Figure 5). Between 0 and  $-10^\circ C$ , the measured magnetization is strongly decreasing and stays constant down to  $-60^\circ C$ , a clear evidence of surface water freezing. The magnetization left at low temperature is due to hydroxyls.

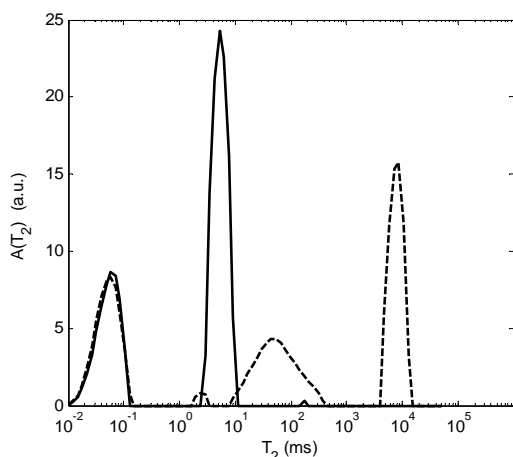


Figure 4:  $D_2O$  exchange experiment on a kaolinite powder initially at 100% relative humidity. Full line: initial state, dashed line: after  $D_2O$  immersion.

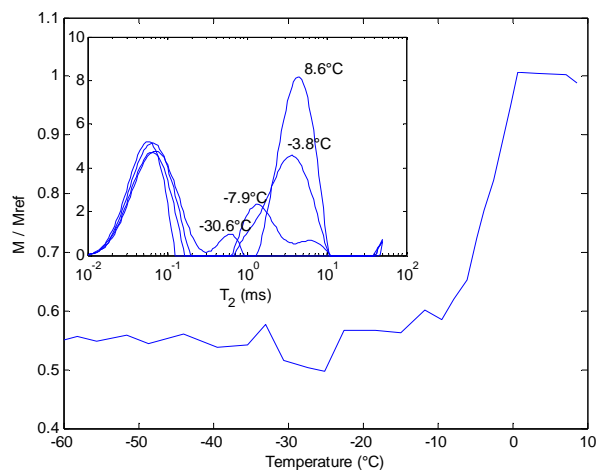


Figure 5: Freezing experiment on a kaolinite powder initially at 100% relative humidity.  $M_0$  is the total magnetization normalized by its value at  $10^\circ C$ .

### Smectite and interlayer signal identification

The  $T_2$  distributions obtained on smectite at 100% relative humidity is typically bimodal (Figure 6 left); the dominant peak is located at about 1 ms ( $T_1/T_2 \cong 1.5$ ), and the second one is at the limit of resolution at 0.06 ms ( $T_1/T_2 \cong 5$ ). There is no obvious signature of the interlayer water, presumably due to the rapid exchange between external and internal water. When considering the smectite powder with ethylene glycol, we observe again a bimodal signature but with inverted proportions: the mode at the smallest  $T_2$  is dominant ( $T_1/T_2 \cong 5$ ) and the other one is shifted down to 0.2 ms ( $T_1/T_2 \cong 1.5$ ) compared to water, similarly to kaolinite. It will be shown later with quantitative evaluations that this peak contains at the same time hydroxyls and ethylene glycol in the interlayer.

We also performed a D<sub>2</sub>O exchange experiment (not shown) that indicated similarly to kaolinite that the  $T_2$  components below 0.1 ms (for RH=100%) can be associated with hydroxyls.

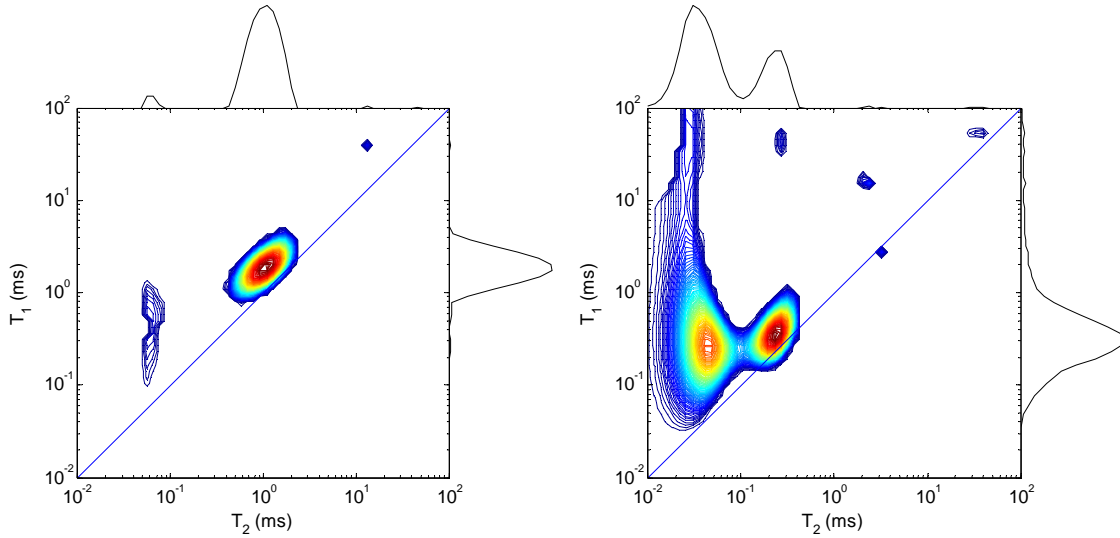


Figure 6:  $T_1$ - $T_2$  maps obtained on smectite powders at 100 % relative humidity using water (left) and ethylene glycol (right).

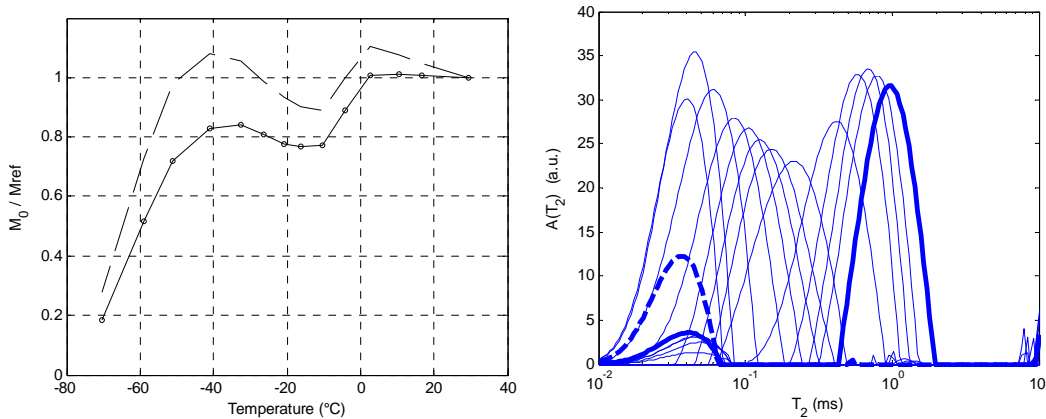


Figure 7: Freezing experiment on a smectite powder at RH=100%. Left: evolution of the total magnetization  $M_0$  normalized by its value at 30°C; dashed line: without a Curie law correction. Right:  $T_2$  distribution obtained at each temperature; thick line: initial temperature (29.4°C), thick dashed line: lowest temperature (-70.4°C). Distribution amplitudes are not corrected for temperature. Inter-echo spacing: 60  $\mu$ s.

The freezing experiment shows clearly the interlayer water (Figure 7). First, the total magnetization  $M_0$  shows two plateau; from 30°C down to 0°C, the magnetization (corrected for temperature) is stable; then, external water is freezing between 0°C and -10°C, resulting in a decrease of about 20 %; from -10 down to -40 °C,  $M_0$  is stable again; the small increase of  $M_0$  is due to the extrapolation method that tends to overestimate  $M_0$

when relaxation components approach the limit of resolution; finally, below  $-40^{\circ}\text{C}$ ,  $M_0$  decreases sharply again. These results are in agreement with the results of Salles et al. [11] who found a solidification temperature of  $-31.2$  and  $-36.7^{\circ}\text{C}$  respectively for homoionic Na and Ca smectites. Second, there is a shift of relaxation times after freezing external water (Figure 7, right), superimposed to a general decrease of relaxation time with temperature. Godefroy et al. [12] have shown that surface relaxivity depends on temperature through surface diffusion mechanisms. At  $-16^{\circ}\text{C}$ , the relaxation time of the interlayer water is at  $0.16$  ms. Selecting all the data between  $-16$  and  $-40^{\circ}\text{C}$ , we can calculate an activation energy (Arrhenius type function) and extrapolate the relaxation time of the interlayer water at  $30^{\circ}\text{C}$ . We find  $0.62$  ms.

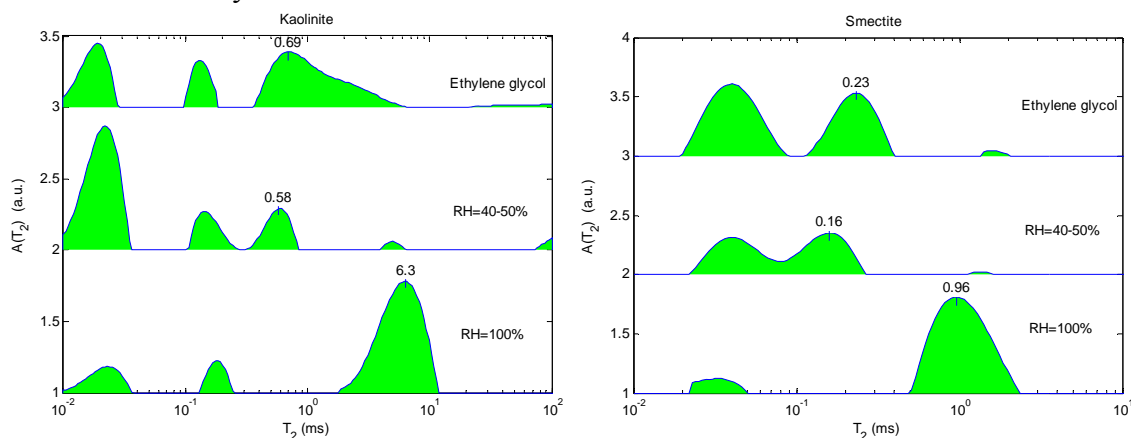


Figure 8:  $T_2$  distribution used for quantitative estimation. The CPMG sequences were measured using a inter-echo spacing of  $30\ \mu\text{s}$ .

### Quantitative aspects

We performed further quantitative evaluation of hydroxyls, external and interlayer water present in different samples. For this, we used a combination of FID and CPMG decays using the  $10\ \text{mm}$  probe and smallest dead times possible; the FID is used to calculate the total measured mass of hydrogen in the sample; the CPMG is used to calculate the amount of liquid at a relaxation time larger than  $0.3$  ms for kaolinite and  $0.1$  ms for smectite. Then, the amount of hydrogen originating from hydroxyls can be calculated from the difference between the total measured hydrogen mass and the measured hydrogen mass from the liquid. It can be compared with the calculated mass of hydrogen with the structural formula, using a dry mass of clay (sample mass minus liquid mass). For kaolinite (Table 3), we found a reasonable agreement, although the amount of hydroxyls is underestimated at  $\text{RH}=100\%$  and ambient humidity. For smectite (Table 3), we have a severe underestimation at  $\text{RH}=100\%$ , and an overestimation for ethylene glycol. In this situation, there is a separation between external and internal liquid due to the low mobility and size of the ethylene glycol molecule.

Once the amount of hydrogen from hydroxyls is subtracted, we can calculate external and internal water or ethylene glycol (EG) in all situations (Table 3). To calculate the amount of internal EG liquid for smectite, we subtracted the theoretical amount of hydrogen from

hydroxyls from the total hydrogen mass. For water at RH=100%, the internal water was calculated at 80% of the total water present in the sample. For water at ambient humidity, we neglect the possible amount of external water. For this case, note the observed relaxation time of 0.16 ms, smaller than interlayer water at RH=100%. The relaxation time of 0.58 ms measured at ambient humidity for kaolinite can be considered as the surface relaxation time  $T_{2s}$ .

Table 3: Quantitative evaluation of the amount of hydrogen and liquid mass (L: water or ethylene glycol) for kaolinite and smectite. IL: interlayer liquid. (\*) the amount of hydrogen is overestimated due to the overlapping of hydroxyls and liquid ethylene glycol below 0.1 ms.

Kaolinite	Sample (mg)	Total H from FID (mg)	H Liquid from CPMG (mg)	H hydroxyls (mg)		mg L/ g clay
				measured	calculated	
			$T_2 > 0.3\text{ms}$			
RH=0 % (100°C)	124.0	2.0		2.0	1.9	
RH=40-50% (ambient)	146.4	1.8	0.2	1.6	2.3	17
RH=100%	138.5	3.2	1.7	1.5	1.9	126
Ethylene glycol	158.3	2.9	0.6	2.3	2.4	42

Smectite	Sample (mg)	Total H from FID (mg)	H Liquid from CPMG (mg)	Interlayer liquid (mg)	H hydroxyls (mg)		mg L/ g clay	mg IL/ g clay
					measured	calculated		
			$T_2 > 0.1\text{ms}$					
RH=0 % (100°C)	124.0	0.5			0.5	0.7		
RH=40-50% (ambient)	259.8	3.3	2.2	19.5	1.1	1.3	81	81
RH=100%	192.3	6.0	5.8	41.8	0.2	0.8	373	298
Ethylene glycol	251.3	5.5	3.0	14.6	2.5 (*)	1.2	220	71

## CONCLUSION

We studied two types of clays, kaolinite and smectite, with different water content, as well as equilibrated with ethylene glycol. At 100°C, the NMR signal at relaxation time smaller than 50  $\mu\text{s}$  is due to hydroxyls forming the crystallographic lattice and the measured and calculated mass of hydrogen agree reasonably well. At 100% relative humidity, kaolinite has a relaxation time of 6 ms, much larger than smectite (1 ms) due to the very large difference of specific surface area. For smectite, the interlayer water is in fast exchange with surface water and cannot be identified at ambient temperature, except when the powder is equilibrated with ethylene glycol, in which case two relaxation modes are present. When freezing the external water, an inter-layer relaxation time  $T_2$  of 0.16 ms can be identified at -16 °C. Using the measured activation energy, the relaxation time of inter-layer water has been evaluated at 0.6 ms at 30°C. At RH=100%, 80% of the detected water is located in the interlayer space. Quantitatively, we were able to calculate the amount of external and internal liquid (water or ethylene glycol) at RH=100% and 40-50% (ambient humidity), and with ethylene glycol. At RH=100%, our results are in

general agreement with Salles et al. [11] on homoionic montmorillonite, in particular for the external/internal water fraction. We found a larger interlayer water content (298 mg/g clay instead of about 200), presumably due to the different smectite used as well as the presence of two cations (Na and Ca). Further work will focus on homo-ionic smectites for detailed comparison with literature data.

## ACKNOWLEDGEMENT

The motivation of this work originates from the TAPSS 2000 research program «Present and past transfers in a sedimentary aquifer – aquitard system : a 2000 meter deep drill-hole in the Mesozoic of the Paris Basin”.

## REFERENCES

- 1 Matteson A., J.P. Tomanic, M.M. Heron, D.F. Allen and W.E. Kenyon, NMR relaxation of clay/brine mixtures, SPE Reservoir Eval. & Eng. (2000) 3-5.
- 2 Michot L.J., F. Villieras, M. François, I. Bihannic, M. Pelletier, J.M. Cases, Water organisation at the solid-aqueous solution interface, C.R. Geoscience (2002) 334.
- 3 Raynal J. and M. Jullien, Experimental and macroscopic evidence of the anomalous state of the water in a clay system, Clay science, (2006) 12 Supplement 2.
- 4 Ben Rhaïem H., Tessier D., Pons C.H., Effect of interlayer cation and relative humidity on the hydration properties of a dioctahedral smectite, Clays Minerals (1986) 21.
- 5 Chitale D.V., J. Gardner and R. Sigal, Significance of NMR  $T_2$  distributions from hydrated montmorillonites, Proceedings of the SPWLA 41<sup>st</sup> Annual Symposium, (2000) paper X.
- 6 Montavon G., Z. Guo, C. Tournassat, B. Grambow and D. Le Botlan, Porosities accessible to HTO and iodide on water-saturated compacted clay materials and relation with the form of water: a low field NMR study, Geochimica et Cosmochimica Acta (2009) 73.
- 7 Bergaya F. and Vayer M., CEC of clays: measurement by adsorption of copper ethylene-diamine complex, Applied Clay Science (1997) 12, 275-280.
- 8 Madejova J., Komadel P. and Cícel B., Infrared study of octahedral site populations in smectites, Clay Minerals (1994) 29, 319-326.
- 9 Besson G. and Drits V.A., Refined relationships between chemical composition of dioctahedral fine-dispersed mica minerals and their infrared spectra in the OH stretching region. Part I: identification of the stretching band, Clays and Clay Minerals (1997) 45, 158-169.
- 10 Moore, D. and R.C. Reynolds, Jr., 1997, X-Ray Diffraction and the Identification and Analysis of Clay Minerals, 2nd ed.: Oxford University Press, New York
- 11 Salles F., O. Bildstein, J.M. Douillard, M. Julien, J. Raynal and H. Van Damme, On the cation dependance of inter lamellar and interparticular water and swelling in smectite clays, Langmuir, (2010) 26-7, 5028-5037.
- 12 Godefroy S., M. Fleury, and F. Deflandre, J.-P. Korb, Temperature effect on NMR surface relaxation, J. Phys. Chem., (2002) 106, 11183-11190.